




# The prevalence of image degradation due to motion in rest-stress rubidium-82 imaging on a SiPM PET-CT system

Ian S. Armstrong, PhD <sup>a</sup>, Matthew J. Memmott, MSc,<sup>a</sup> Charles Hayden, MSc,<sup>b</sup> and Parthiban Arumugam, MD<sup>a</sup>

<sup>a</sup> Nuclear Medicine, Manchester University NHS Foundation Trust, Manchester, UK

<sup>b</sup> Siemens Medical Solutions USA, Inc., Molecular Imaging, Knoxville, TN

Received Nov 5, 2020; accepted Jan 7, 2021

doi:10.1007/s12350-021-02531-y

**Background.** Motion of the heart is known to affect image quality in cardiac PET. The prevalence of motion blurring in routine cardiac PET is not fully appreciated due to challenges identifying subtle motion artefacts. This study utilizes a recent prototype Data-Driven Motion Correction (DDMC) algorithm to generate corrected images that are compared with non-corrected images to identify visual differences in relative rubidium-82 perfusion images due to motion.

**Methods.** 300 stress and 300 rest static images were reconstructed with DDMC and without correction (NMC). The 600 DDMC/NMC image pairs were assigned Visual Difference Score (VDS). The number of non-diagnostic images were noted. A “Dwell Fraction” (DF) was derived from the data to quantify motion and predict image degradation.

**Results.** Motion degradation (VDS = 1 or 2) was evident in 58% of stress images and 33% of rest images. Seven NMC images were non-diagnostic—these originated from six studies giving a 2% rate of non-diagnostic studies due to motion. The DF metric was able to effectively predict image degradation. The DDMC heart identification and tracking was successful in all images.

**Conclusion.** Motion degradation is present in almost half of all relative perfusion images. The DDMC algorithm is a robust tool for predicting, assessing and correcting image degradation. (J Nucl Cardiol 2022;29:1596–606.)

## Abbreviations

DDMC	Data-driven motion correction
DF	Dwell fraction
DVH	Direct volume histogram
NAC	Non-attenuation-corrected
NMC	Non-motion-corrected

PET	Positron emission tomography
TOF	Time-of-Flight
VDS	Visual difference score

## See related editorial, pp. 1607–1610

**Supplementary Information** The online version of this article (doi:<https://doi.org/10.1007/s12350-021-02531-y>) contains supplementary material, which is available to authorized users.

This article includes a PowerPoint file that should be made available as ESM on SpringerLink. Please include the standard Springer ESM text in the note/footer on the first article page.

The authors of this article have provided a PowerPoint file, available for download at SpringerLink, which summarizes the contents of the

paper and is free for re-use at meetings and presentations. Search for the article DOI on SpringerLink.com.

Reprint requests: Ian S. Armstrong, PhD, Nuclear Medicine, Manchester University NHS Foundation Trust, Oxford Road, Manchester; [Ian.Armstrong@mft.nhs.uk](mailto:Ian.Armstrong@mft.nhs.uk)

1071-3581/\$34.00

Copyright © 2021 American Society of Nuclear Cardiology.

## INTRODUCTION

Motion of the heart during stress and rest PET acquisition has been shown to introduce a varying degree of non-uniform blurring in the reconstructed images; hampering image interpretation and, in extreme cases, rendering the images either non-diagnostic or leading to incorrect interpretation.<sup>1-4</sup> As developments in scanner technology continue, the degrading impact of motion on the static relative perfusion images is more apparent and hence the correction for this becomes ever more important. New PET-CT systems that employ Silicon Photomultipliers (SiPM) for signal detection offer a significant increase of performance over systems that use traditional photomultipliers. The improved time-of-flight (TOF) performance, sensitivity and spatial resolution produces a notable improvement to image definition for rubidium-82 images meaning that motion blurring becomes a more prominent source of image degradation. Therefore, it is not surprising that motion correction has been highlighted as an increasingly relevant consideration.<sup>5</sup>

Excluding cardiac contraction, there are two forms of heart motion that will give rise to motion blurring in perfusion images: oscillation, either periodic or irregular, in the position of the heart about a given baseline position and a gradual drift in the position of this baseline. It has been shown that the types of motion observed in rest-stress cardiac PET are diverse, supporting the development of a dedicated motion correction technique.<sup>1</sup> We have previously demonstrated the utility of a prototype data-driven motion correction (DDMC) algorithm, developed by Siemens Medical Solutions as part of a research collaboration, that provides high temporal resolution motion tracking and correction of image blurring in static relative perfusion images.<sup>1</sup> The findings from our preliminary work demonstrated a clear benefit of the DDMC algorithm for clinical cases and how motion blurring affected image interpretation.<sup>1</sup> All the images that were considered non-diagnostic as a result of motion blurring were salvaged and interpretable following DDMC. This raises obvious follow-on questions: firstly, just how often does motion of the heart produce an appreciable visual impact in routine imaging? Secondly, what degree of motion is necessary to produce a visually perceivable effect?

To date, studies evaluating motion in cardiac PET are divided into two categories. The first being studies focusing on respiratory motion gating where motion tracking is performed either by data-driven or external trigger methods. These have been small scale and selective examples<sup>6-8</sup> with some being conducted with image acquisition for patients in a resting state only. The second category of studies have focused on motion in

dynamic cardiac PET imaging for myocardial blood flow calculation.<sup>9-14</sup> While this second study type provides an insight into motion during rest and stress imaging, the inherent nature of simply assessing frame-to-frame shifts, and largely neglecting intra-frame motion blurring, may not fully illustrate the impact of motion on static relative perfusion images averaged over several minutes.

To date there is limited literature on the visual assessment of motion in cardiac PET. Vleeming et al. performed a visual appraisal with a 3-category grading for ammonia stress static perfusion images from a cohort of 61 patients without motion correction.<sup>15</sup> In a preliminary evaluation of the DDMC algorithm for this work, we have previously performed a 4-category grading of motion for images before and after motion correction.<sup>1</sup> These images were preselected based on an inclusion criterion of perceived motion artifacts on the non-corrected images. Hence, we believe that no studies to date have visually assessed the degradation of images due to motion blurring in a large number of consecutive routine rubidium-82 rest and stress studies.

In this study, we aimed to evaluate the impact of motion blurring of varying degrees over a large number of consecutive studies in order to determine the prevalence of image degradation due to motion in rubidium-82 cardiac PET. We also aimed to demonstrate the prevalence of non-diagnostic images due to excessive motion blurring. Visual differences were recorded for images with and without a recently developed prototype DDMC algorithm.<sup>1</sup> We used the DDMC algorithm to track the position of the heart with 1 mm precision and a temporal resolution of 1 second. Motion traces were produced and used to derive a novel figure of merit to quantify the motion and predict the degree of visual image degradation.

## METHODS

### Data-Driven Motion Correction

The DDMC algorithm implemented in this work is the same as described previously.<sup>1</sup> Briefly, coincidence events are binned directly from the listmode PET data into a volume, rather than sinograms, by utilizing the TOF information. These volumes are referred to as a Direct Volume Histogram (DVH). One DVH frame is created for every one second of coincidence events collected hence there are 300 DVH frames created over the entirety of the 5-minute listmode acquisition. The heart is located within each DVH frame and its displacement, relative to a reference position, is tracked with 1 mm precision. From here, displacement markers are inserted into the listmode data at 1-second intervals

**Table 1.** Patient demographics for this study

Total number patients	300	
Gender	181M; 119F	
Age (years)	65 [9] (56–73)	
Median [MAD] (IQR)		
Weight (kg)	85 [15] (72–102)	
Median [MAD] (IQR)		
Height (m)	1.68 [.07] (1.60–1.74)	
Median [MAD] (IQR)		
BMI (kg/m <sup>2</sup> )	30.5 [4.5] (26.4–35.9)	
Median [MAD] (IQR)		
Resting systolic BP	128 [14] (114–142)	
Median [MAD] (IQR)		
Resting heart rate	70 [10] (60–80)	
Median [MAD] (IQR)		
Stress agent	Adenosine	266
	Regadenoson	34

Values are shown as median, median absolute deviation [MAD] with inter-quartile range (IQR)

for reconstruction. Currently this is only performed in the *z* (axial) direction.

### Patient Selection and Image Acquisition

600 static relative perfusion images (300 stress and 300 rest) from 300 consecutive patients over a 2-month period who underwent a clinically indicated rubidium-82 perfusion scan were retrospectively included in this study. The patient demographics from these cases are given in Table 1. A Shapiro-Wilk test for normality of all continuous variables was performed and all data were found to be not normally distributed so are quoted as median, median absolute deviation and inter-quartile range. All images were fully anonymized prior to reconstruction and analysis.

All patients were required to abstain from caffeine for 12 hours prior to imaging. A single low-dose CT scan (120 kV; 11 mAs quality reference with CARE-Dose modulation) was acquired for attenuation purposes. This was followed by a rest-stress protocol with 740 MBq (20 mCi) of rubidium-82 administered for both rest and stress. A 5-minute listmode acquisition acquired on a Siemens Biograph Vision 600 (Siemens Medical Solutions USA, Inc.) was started as the rubidium-82 was administered. Pharmacological vasodilator stress was used in all patients, with the choice of agent shown in Table 1. The choice of vasodilator stress agent in our institution depends on several factors including cost, co-morbidities (severity of airways disease, aortic stenosis, etc.) and patient weight. The administration

protocol for the stressing agents is the same as our previous work evaluating DDMC.<sup>1</sup> Adenosine was infused for 4.5 minutes at 140 µg/min/kg with the rubidium infusion commencing 2 minutes after the start of the adenosine infusion. A fixed 400 µg dose in 5 mL of regadenoson was administered slowly over 20 seconds and followed by a 5 mL saline flush administered over 10 seconds. The rubidium infusion was started 60 seconds after the saline flush was given. All patients were positioned with both arms raised above their head, with arms supported by a Velcro strap. In addition, a wide Velcro strap was wrapped around the patients' upper abdomen to minimize voluntary patient movement on the imaging couch.

### Image Reconstruction

Listmode PET data without and with motion correction were framed into 180 second sinograms over the time range of 120 to 300 seconds after the start of the scan. From here, static relative perfusion images were reconstructed without motion correction (NMC) and with motion correction (DDMC). In both cases, any adjustment translation in PET to CT registration was obtained from a non-attenuation-corrected PET image. Images were reconstructed with all relevant corrections using a 3D OSEM iterative reconstruction algorithm incorporating both TOF and point spread function modeling with 4 iterations, 5 subsets and a 6.0 mm FWHM Gaussian post-filter. The matrix was 220 × 220 with a zoom of 2.0 and 159 transaxial slices giving voxel dimensions of 1.6 × 1.6 × 1.6 mm<sup>3</sup>.

### Image Interpretation

The 600 images were shown as pairs (NMC and DDMC) to two observers (IA, MM) in the format of short, horizontal and vertical long axis slices obtained from Cedars Sinai QPET (Cedars Sinai, Los Angeles, CA, United States). All images were blinded, to the extent that the observers did not know which image was NMC and which was DDMC, and randomized. The two observers were asked to define a Visual Difference Score (VDS) of 0, 1 or 2, which represented the following: 0: no difference perceivable between the images; 1: a subtle difference perceivable between the images and 2: a clear difference between the images. Areas that the observers were asked to take note of were homogeneity and intensity of uptake in the myocardium, separation between the myocardium and surrounding extra-cardiac activity and clarity of the ventricular cavity. Figure 1 gives examples of image pairs rated a VDS of 1 and 2. Following assessment by the two observers, any differences in VDS classification across

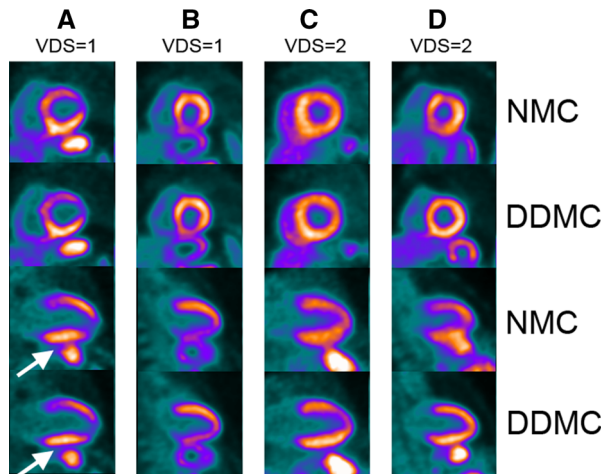


**Figure 1.** Demonstration of characteristics that were used to attribute the corresponding visual difference scores (VDS) for non-motion-corrected (NMC) compared with the motion-corrected images (DDMC). Image pair (A) shows subtle improvement to the separation of the inferior wall from extra-cardiac activity; image pair (B) shows subtle improvement to the inferior wall intensity; image pairs (C) and (D) show clear improvement to the overall definition and intensity of the myocardium, while image pair (D) also shows clear improvement of the separation of the inferior wall from extra-cardiac activity.

image pairs were discussed jointly and a consensus score was assigned to produce a single table of values.

### Clinical Assessment

Images pairs with a VDS of 2 are indicative of cases where motion has produced a substantial visual impact on the NMC images. To assess the impact of this motion on interpretation and quantify the prevalence of non-diagnostic images, the NMC images from these image pairs were then graded by a nuclear medicine physician (PA) according to image quality as good, adequate or non-diagnostic. The corresponding DDMC images were then also assessed to determine any change in image quality. Given that each study comprises of both a rest and stress image, the proportion of the 300 studies considered to be non-diagnostic based on the rest, stress or both NMC images being graded as non-diagnostic was determined.

### Motion Quantification

**Motion traces** The DDMC algorithm generates a trace, with 1 second and 1 mm precision, of the heart displacement in the  $x$ ,  $y$  and  $z$  axes relative to the position of the heart in the DVH reference frame. The choice of the reference DVH frame is arbitrary and primarily based on good visualization of the heart such

that the blood-pool activity has cleared. In the DVH reference frame, the position of the heart could occur at any point over the local range of motion that it undertakes. To compensate for this, the displacement trace is adjusted so that the vectors are set relative to the average position of the trace, rather than the DVH reference frame, over the temporal framing of the static relative perfusion image. This is illustrated in Figure 2A where the position of the heart in frame 180—the DVH reference frame—can be seen to be at a local peak of the motion trace and hence the overall trace has a negative offset, which is compensated and shown in Figure 2B. To allow comparison with our preliminary evaluation, the mean absolute displacement of the heart in the  $x$ ,  $y$  and  $z$  axes was determined from the motion traces for each VDS category.

**Figure of merit** We have previously evaluated four figures of merit derived from the  $z$ -axis motion trace to predict the visual impact of motion.<sup>16</sup> These were the cumulative absolute displacement, the standard deviation of the displacement vectors, the total “distance traveled” by the heart and the “Dwell Fraction”. From this preliminary work, the “Dwell Fraction” (DF) was shown to provide superior quantification and prediction of the degree of visual motion degradation. To describe DF, one can consider the final reconstructed image as a composite image of the heart from the discrete 1-second time intervals throughout the acquisition. Image quality will be maximized when the position of the heart is consistent throughout these intervals. Reduction in this consistency will lead to image degradation. The quantification of this therefore is two-fold: firstly, the position that the heart dwells in the most is calculated and secondly the fraction of time spent within a window centered on this dwell position provides us with the quantitative measure. An important consideration is the decay of rubidium-82, with the data contribution to the final image reducing in statistical quality over time. To this end each displacement vector of the heart, relative to the DVH reference, is weighted according to radioactive decay.

Each motion trace contains 180 displacement vectors of the heart relative to the reference position across the 180 second framing of the static relative perfusion images. A spatial window, referred to as a dwell window, of discrete width is superimposed on the motion trace and the proportion of the displacement vectors within the window is calculated. The dwell window center position is incremented from the minimum to maximum displacements within the motion trace to determine the dwell window location that maximizes the number of displacement vectors within the window. The DF figure of merit is hence defined as the fraction of the 180 displacement vectors that fall

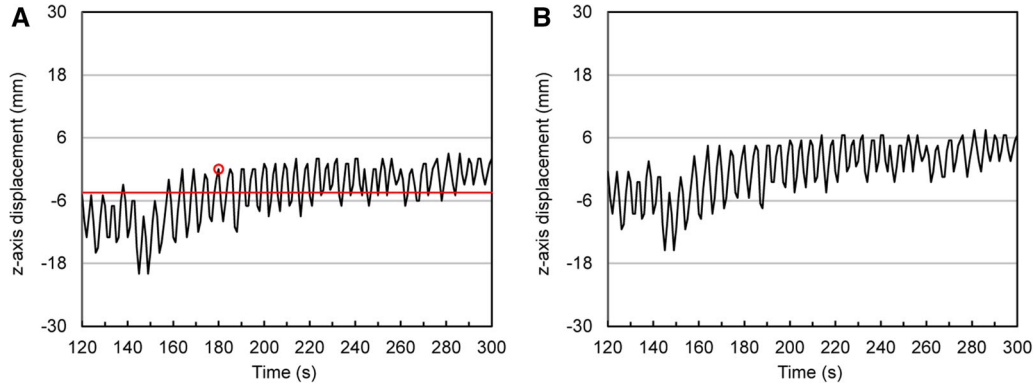


**Figure 2.** (A) Example original motion trace where displacement is relative to the reference DVH frame at 180 seconds (highlighted by red circle). The average position of the trace is  $-4.5$  mm, which is shown by the red line. (B) The same trace now shown with displacement relative to the average position. The trace here represents the motion in the  $z$ -axis (axial) displacement.

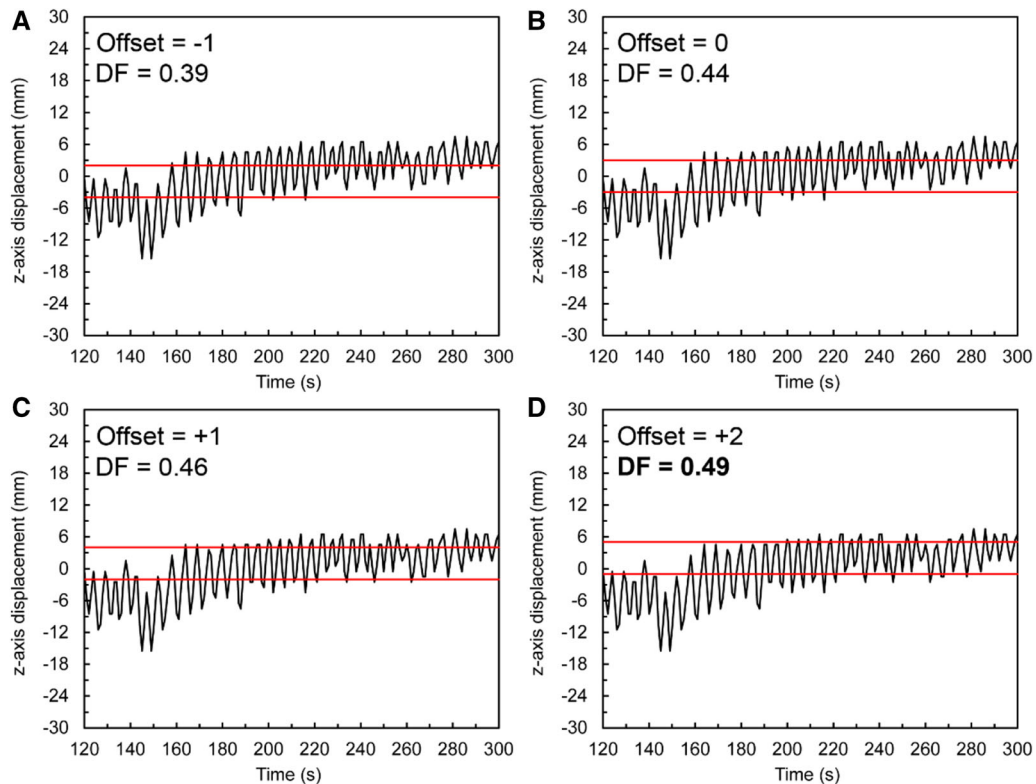


**Figure 3.** Displacement traces in the  $z$  (axial) direction, corrected for the average position of the heart (as shown in Figure 1B) with the position of the dwell window (red lines) shown with offsets of (A)  $-1$  mm with limits  $-4$  to  $+1$  mm; (B)  $0$  mm with limits  $-3$  to  $+3$  mm; (C)  $+1$  mm with limits  $-2$  to  $+4$  mm and (D)  $+2$  mm with limits  $-1$  mm to  $+5$  mm. The dwell fraction (DF) is calculated for each plot and shown but it is the window offset of  $+2$  mm that maximizes the dwell fraction with a value of .49 and it is this value that is recorded for this motion trace.

within this optimal dwell window position. Figure 3 demonstrates this for a dwell window width of 6 mm and various offsets. In the figure, it is shown that, despite the trace being corrected for average position, an offset of + 2 mm for the dwell window maximizes the DF, as shown in Figure 3D. For a given camera technology and tracking algorithm, the dwell window width must be optimized as this will be dependent on the intrinsic resolution of the DVH images used in identifying the location of the heart, hence dwell window widths of 1 to 22 mm were evaluated. DF was calculated independently in the *x*, *y* and *z* directions and the dwell window width was equal in each direction.

### Statistical Analysis

SPSS version 23 (IBM Corp, Armonk, NY) was used for statistical analysis. The VDS categories for stress and rest images were compared using a Chi-Squared test. A Shapiro-Wilk test was performed on continuous data, which determine no data were normally distributed. Consequently, non-parametric Mann-Whitney *U*-Tests were performed to compare the distributions of groups of data and, after a Bonferroni correction for multiple comparisons, a *P*-value of .004 was used to identify significant differences in the distributions of each group.

Receiver operating characteristic (ROC) analysis was performed on the DF to distinguish between the VDS categories. The area under the ROC curve was calculated to distinguish clear motion degradation (VDS = 0 vs VDS = 2) and any motion degradation (VDS = 0 vs VDS = 1 or 2). The window width used in the DF calculation was optimized by repeating the ROC analysis for widths of 1 to 22 mm. Standard Errors (SE) were determined using an implementation of DeLong’s non-parametric approach.<sup>17</sup> For graphical purposes, ROC confidence intervals were generated using a bootstrapping approach with replication.

## RESULTS

### Visual Differences

Table 2 shows the distribution of the VDS categories for the study, with data separated into rest and stress images. The data show a greater prevalence of image degradation due to motion for stress images compared with rest (*P* < .001). For the 36 cases with a VDS of 2, the clinical image quality scores for the NMC images were adequate for 29 images and non-diagnostic for 7 images (5 stress and 2 rest). In all but one case, these images were part of separate studies indicating that 6 of the 300 studies were non-diagnostic as a direct consequence of motion affecting one or both images within a study. All but two of the corresponding DDMC images were rated as good quality, with the remaining two images being rated adequate due to high patient BMI producing low-count images—hence not related to motion. In these 36 cases, quality was improved in 34 and unchanged in 2. Figure 4 shows the image quality scores assigned to both the NMC and the DDMC images to indicate differences in the scores for given image pairs.

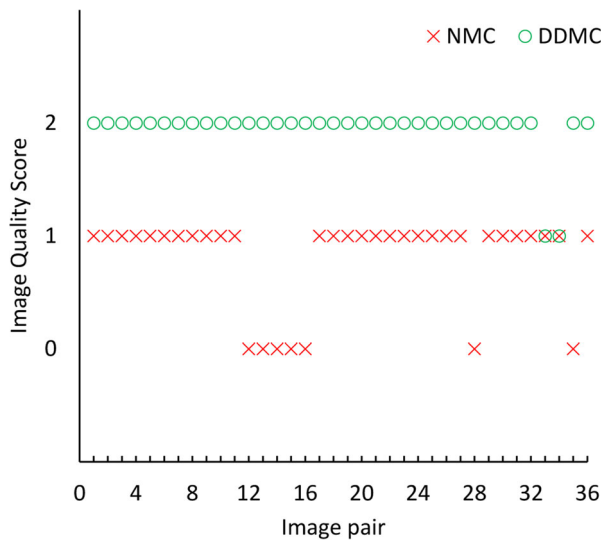
### Motion Quantification

Figure 5 shows histograms of the mean absolute displacement of the heart in the *x*, *y* and *z* directions for each VDS category. The plot where VDS = 2 can be compared with the results of our preliminary evaluation of DDMC<sup>1</sup> which, by definition, consisted of images that would also have had a VDS of 2 as the cases were selected based on clear motion blurring. The plots in Figure 5 clearly show an increasing mean displacement along the *z* direction with increasing VDS. There appears to be very little difference in the mean displacement in either the *x* or *y* directions across the three VDS categories.

The DF distribution measured at rest was not found to be significantly different from the distribution at stress within the same VDS category. Consequently,

**Table 2.** Consensus of visual difference scores (VDS) categories of image difference shown for rest and stress, with stress results also separated into stress agent

VDS	Rest [N (%)]	All stress [N (%)]	Adenosine stress [N (%)]	Regadenoson stress [N (%)]	Total [N (%)]
0	200 (66.7%)	127 (42.3%)	114 (42.9%)	13 (38.2%)	327 (54.5%)
1	92 (30.7%)	145 (48.3%)	127 (47.7%)	18 (52.9%)	237 (39.5%)
2	8 (2.7%)	28 (9.3%)	25 (9.4%)	3 (8.8%)	36 (6.0%)



**Figure 4.** Image quality scores of the 36 image pairs assessed by a clinician where a visual difference score of 2 was defined. Quality scores are 0: non-diagnostic, 1: adequate and 2: good. NMC: non-motion-corrected; DDMC data-driven motion correction.

stress and rest data were combined to assess statistical differences in the DF distribution for each VDS category and in each direction. Figure 6 shows box plots of DF grouped by VDS category to illustrate the differences seen in across the three directions of motion. As shown in the figure, the DF distribution is consistently lower in  $z$  (axial) direction compared with the  $x$  or  $y$  directions irrespective of the VDS category. Interestingly, a significant difference was seen for the distribution of DF in the  $x$  and  $y$  directions for the VDS = 0 category. This is due to the very narrow distribution in the  $y$ -direction. After combining stress and rest data, the median values of DF for VDS = 0 category were .967, .989 and .811 in the  $x$ ,  $y$  and  $z$  directions respectively; for the VDS = 1 category the median values were .939, .944 and .594 in the  $x$ ,  $y$  and  $z$  directions respectively and for the VDS = 2 category the median values were .817, .878 and .422 in the  $x$ ,  $y$  and  $z$  directions respectively. Figure 7 shows the same distributions of DF grouped by direction to illustrate the differences seen in across the three VDS categories. Significant differences were seen in the DF distribution between each VDS category in all directions.

### ROC Analysis

The optimal dwell window width that maximized the AUC for the ROC curve in the cohort was 6 mm (i.e., window center  $\pm 3$  mm), as shown in Figure 8A. It should be noted that this width is applicable to data acquired on the Biograph Vision; other widths may be

optimal on different scanners. Using this value, the AUC (SE) for clear motion degradation (VDS = 0 vs VDS = 2) was .997 (.002) and to distinguish any motion degradation (VDS = 0 vs VDS = 1 or 2) the AUC (SE) was .937 (.009). Figure 8B shows the ROC curves for this data. Figure 9 shows a pictorial representation of the VDS classification, comparing the fraction of each VDS category as a function of DF. It can be seen that a DF greater than .9 indicates good data, a DF of .6 to .9 has an increasing probability of moderate motion giving rise to an adequate quality scan and a DF less than .6 would indicate an increasing likelihood of poor resultant image quality and impairment on interpretation.

### DISCUSSION

In this study, we have visually assessed 600 rubidium-82 static relative perfusion images reconstructed with and without a prototype DDMC algorithm and compared them visually for differences where correction was performed to motion along the axial direction only. By comparing corrected and non-corrected images we have demonstrated, through categorization of perceived visual differences, the prevalence of image degradation by motion. Motion traces in three dimensions, with 1 second and 1 mm precision, of all images were produced over the 180 second time course of the static relative perfusion images. From here, a ‘‘Dwell Fraction’’ figure of merit was derived and can be extracted from the raw listmode PET data prior to reconstruction. This can be used as a predictor of image degradation. Finally, we have demonstrated the proportion of studies that are non-diagnostic as a result of one or both of the NMC image sets being non-interpretable due to motion. We believe this to be the first study of its type that has evaluated the prevalence of motion, utilizing non-corrected and corrected images, in rest-stress rubidium cardiac PET using such a method.

To our knowledge, the only other study to characterize visual motion degradation in cardiac PET is by Vleeming et al.<sup>15</sup> Their study assessed 61 stress (30 with adenosine and 31 with regadenoson) static relative perfusion images acquired using ammonia. Images were reviewed and a consensus rating of small, intermediate or large was assigned in respect to perceived motion artifacts. They reported artifacts in 14/30 (46.7%) adenosine cases (12 small and 2 intermediate) and 9/31 (29.0%) regadenoson cases (all of which were small). No large artifacts were seen for either stress agent. The crucial difference in their work and the visual assessment in our study is that they did not have motion-corrected images to compare against and so it is quite likely some images may have contained some degree of

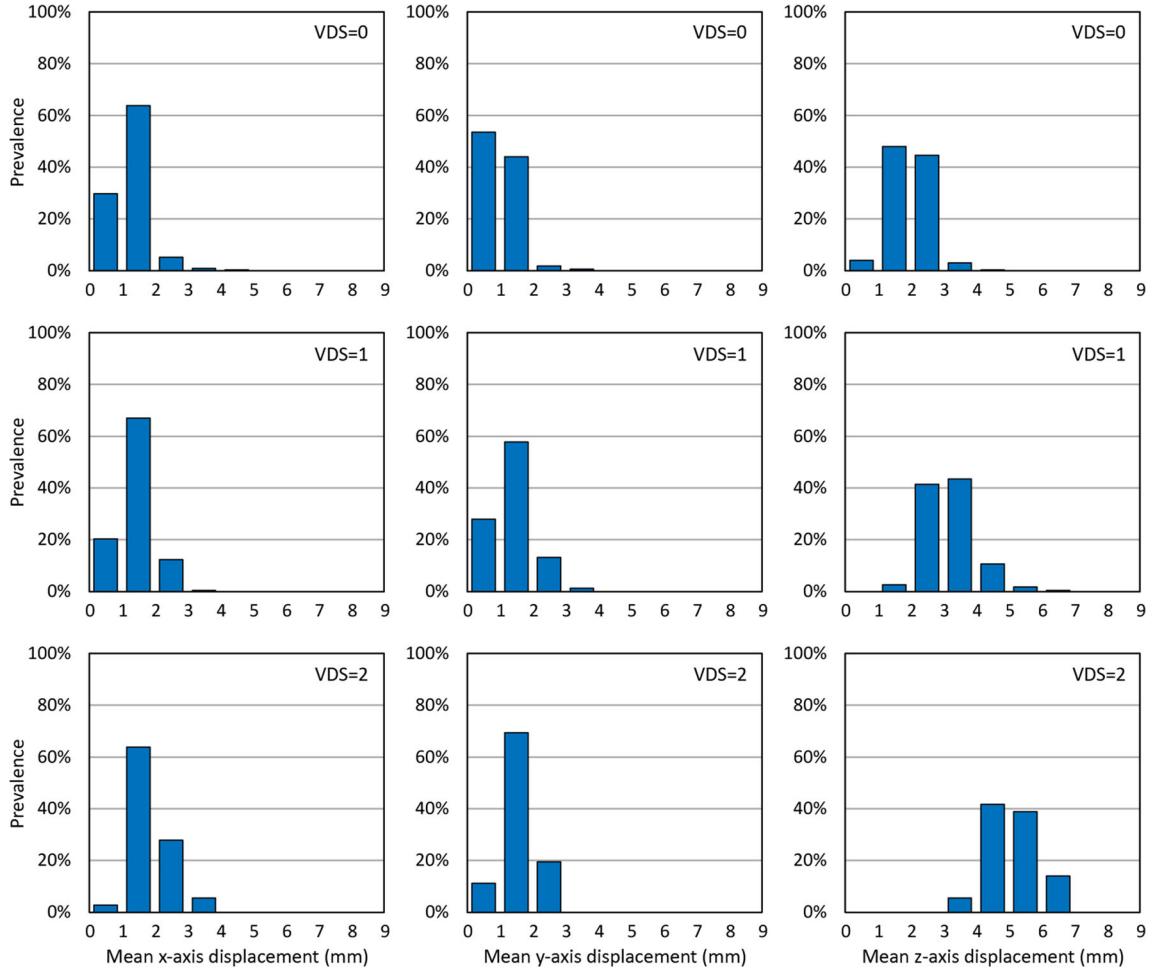


**Figure 5.** Histograms of the mean absolute displacement of the heart in the *x* (left column), *y* (center column) and *z* (right column) directions for each visual difference score (VDS) category. The number of images in each bin has been normalized as a percentage of the total number of images in each VDS category and rest and stress data have been combined in each VDS category.

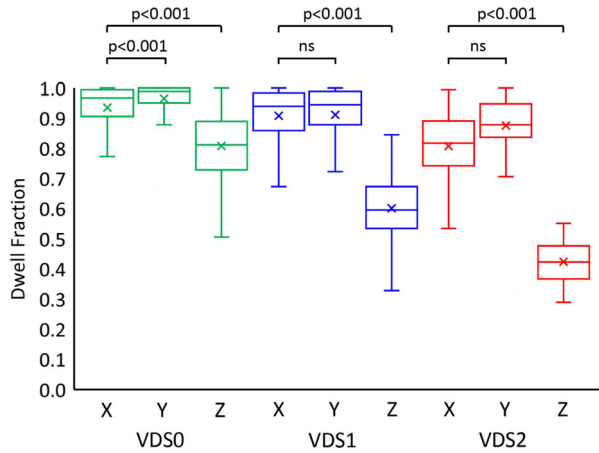


**Figure 6.** Boxplots of the dwell fraction (DF) in the three dimensions for each visual difference score (VDS) category; *ns* not significant.

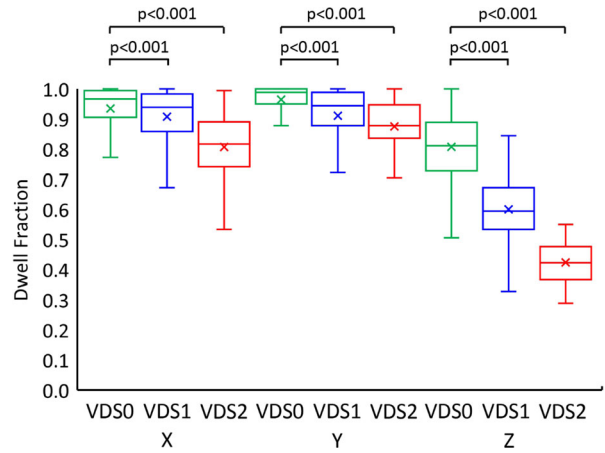


**Figure 7.** Boxplots of the dwell fraction (DF) across the visual difference score (VDS) categories for each direction of motion.



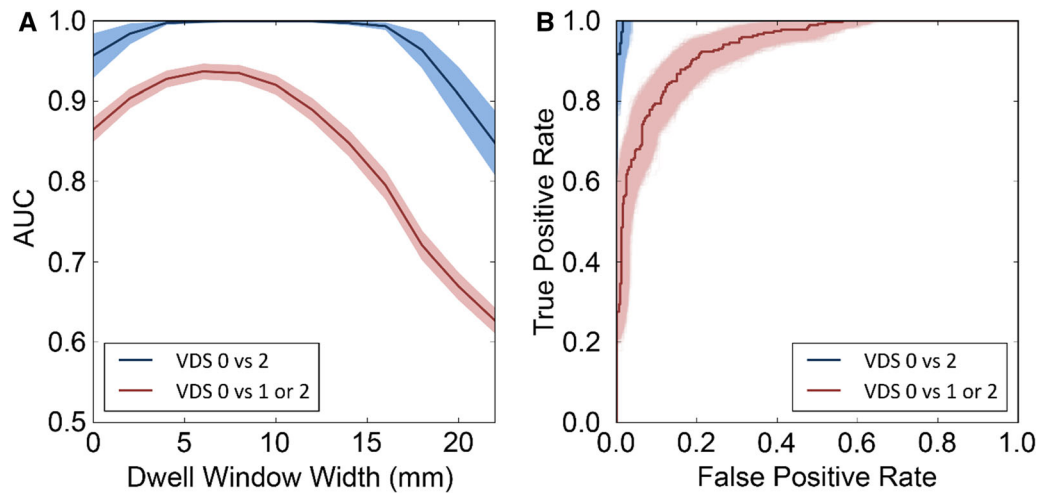


**Figure 8.** (A) Area under curves (AUC) values from the ROC analysis using a range of dwell window widths in the dwell fraction calculation. (B) ROC curves using the optimal window width of 6 mm (window center  $\pm$  3 mm) giving AUC of .997 for VDS = 0 vs VDS = 2 (blue line) and .937 for VDS = 0 vs VDS = 1 or 2 (red line). Shading regions in both figures represent 95% confidence intervals.

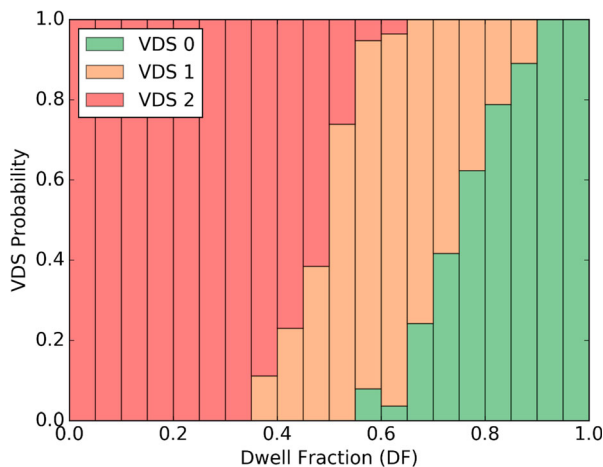


**Figure 9.** Pictorial representation of how the dwell fraction (DF) can be used as a predictor of the VDS category and hence image degradation in the non-motion-corrected images. A smooth transition in probability can be seen between categories. A DF of less than .9 would indicate an increasing probability of motion and less than .6 would indicate a likely degradation of image quality and an impairment on interpretation.

motion blurring but were considered normal. Of course, the differences between the definitions of a motion “artifact” and motion “degradation” are quite subjective. One may argue an artifact may lead to incorrect interpretation while degradation may simply reduce the overall image quality.

A greater prevalence of motion degradation was observed in stress images with 58% of images showing

visual differences compared with 33% of rest images. This is not surprising due to the uncomfortable side-effects of pharmacological stress agents and is in line with studies that have evaluated frame-by-frame motion in rest-stress dynamic scans.<sup>11-13</sup> Adenosine and regadenoson were both used as stress agents in this study. The proportional split of cases into the three VDS categories is similar for either stress agent. However, due to the small number of patients stressed with regadenoson, it is difficult to draw robust comparisons with the degree of motion degradation seen in the patients stressed with adenosine. Other studies have evaluated the degree of motion for these two agents and have reported less motion with regadenoson.<sup>12,15</sup>

We have previously demonstrated the benefit of the prototype DDMC algorithm on images that were seriously degraded by motion blurring<sup>1</sup> but, until now, we have been blind to the proportion of images that suffer from subtle motion degradation. In our preliminary work, we have acknowledged that a current limitation of the DDMC prototype is the correction in the axial direction only. Consequently, one could argue that perceived visual differences recorded in this work would be greater if images were corrected for motion in all three directions. However, the heart tracking in the algorithm has shown that the magnitude of motion along the axial direction is substantially greater than that observed in the transaxial directions and so we would foresee any differences to be small in comparison to correcting in the axial direction only.

Studies that have quantified the magnitude of motion fall into two categories. Firstly, there are those based on respiratory gating techniques consisting of assigning data into one of several discrete positional bins based on the respiratory motion trace. The second category is dynamic studies that track frame-by-frame translations relative to a reference frame. For the dynamic studies, the temporal resolution is limited by dynamic framing duration and hence it is difficult to directly compare results to those presented here. Those studies that have quantified the magnitude of motion based on respiratory gating will, by definition, be limited to assessing the displacement of the heart across the discrete respiratory gated cardiac images. A study by Lassen et al on a cohort of seven patients employed a similar data-driven cardiac detection and correction technique to our study but binned 10 minutes of listmode data into four amplitude-based gated images.<sup>7</sup> They reported the maximum displacement between each gate and the reference gated image and observed a mean axial displacement of  $23 \pm 8$  mm and mean transaxial displacement of  $17 \pm 7$  mm in ammonia scans. Büther et al. extracted a respiratory motion signal by Fourier filtering of a motion trace extracted from 20 minutes of listmode data in 29 patients.<sup>6</sup> From here, they binned data into eight amplitude-based gated images and reported the displacement of the myocardium between the maximum inspiration and maximum expiration gates. They reported displacement of  $9.4 \pm 4.5$  mm which is assumed to be the absolute vector and not solely attributed to the axial direction. Dawood et al employed a more traditional optical respiratory gating approach in seven patients and binned 20 minutes of listmode data into 8 gates.<sup>8</sup> They reported axial displacement ranging from 6 to 27 mm. It should be noted that the duration of data acquisition from these studies is notably longer than the 3 minutes used in this study. As discussed, we have previously evaluated a range of figures of merit derived from the motion trace, which included the summed absolute displacement and the “distance traveled”, defined as the sum of the differential of the displacement.<sup>16</sup> However, the dwell fraction (DF) was found to give the best predictor of visual motion degradation.

The DF figure of merit can be derived from the listmode PET data. This can be used to inform the reporting clinician about the probability that the images have been degraded by motion, and to what extent the degradation may be. This would be useful for cases where images appear suboptimal but there is an uncertainty on the root cause of image degradation. The DF value could be used to recommend the use of motion correction to improve image quality.

Traditional respiratory gating using external trigger devices measure the changing amplitude of a sensor,

which may be the position of a reflective marker for optical systems or diameter of expanding belts placed around the patient. They assume correlation between the external markers and internal organ movement, which may not always be the case. Alternative data-driven techniques have been proposed to counter the shortcomings of these external trigger methods. One recent study has suggested positron-emitting fiducial markers placed on the patient’s abdomen.<sup>18,19</sup> The authors demonstrated the failure of the gating with traditional trigger techniques in several patients. They showed that the fiducial marker technique offered a convenient setup but noted that care must be taken during setup to ensure optimal placement of these markers. In our study, the heart was correctly localized and tracked by the DDMC algorithm in all 600 images demonstrating the robustness of the algorithm.

### Limitations

The current implementation of the DDMC algorithm only corrects motion in the z (axial) direction and, as mentioned, one could argue that the visual comparison of the NMC and DDMC images in this study underestimates the visual degradation that occurs due to motion. However, as we show here, the motion is predominantly in the axial direction and hence we expect any differences to be small by comparison. The clinical assessment of image quality was only performed for image pairs with a clear difference in appearance ( $VDS = 2$ ) and not subtle differences ( $VDS = 1$ ). This was to show the utility of the DDMC algorithm to recovery images most affected by motion. Based on the results here, and our previous evaluation,<sup>1</sup> we would not expect any degradation of image quality after DDMC. This study was performed as a retrospective analysis, without clinical follow-up, and was designed to demonstrate the prevalence of motion that occurs in a routine service. It was not intended to demonstrate the ability of the DDMC algorithm to provide more clinically accurate results. Future work is planned with clinical correlation to assess this.

### NEW KNOWLEDGE GAINED

We believe that this is first study of its type to demonstrate the prevalence of image degradation of static relative perfusion PET images as a direct result of motion blurring by visual assessment and scoring based on comparison of non-corrected and corrected images. While the prevalence of non-diagnostic images is low, almost half of all images are degraded to some extent by motion. By utilizing a newly-developed data-driven motion correction algorithm, a figure of merit has been

proposed, which can be derived from the listmode data, as a predictor of motion degradation.

## CONCLUSION

In this study, we have demonstrated the prevalence of image degradation of rubidium-82 cardiac images due to motion blurring. Motion degradation is more apparent in stress images with 58% of stress images showing evidence of motion compared with 33% of rest images. A “dwell fraction” figure of merit has been proposed which can be used to give a probability of the degree of image degradation as a result of motion blurring. This work has continued from our previous preliminary evaluation of the prototype DDMC algorithm and has shown to be robust on a large number of cases.

## Disclosure

*Charles Hayden is a full-time employee of Siemens Medical Solutions Inc. USA. Ian S. Armstrong, Matthew J. Memmott and Parthiban Arumugam have no conflicts of interest to disclose.*

## References

1. Armstrong IS, Hayden C, Memmott MJ, Arumugam P. A preliminary evaluation of a high temporal resolution data-driven motion correction algorithm for rubidium-82 on a SiPM PET-CT system. *J Nucl Cardiol.* 2020. <https://doi.org/10.1007/s12350-020-02177-2>.
2. Arasaratnam P, Al-Zahrani A, Wells RG, Beanlands RSB, deKemp RA. Respiratory motion resulting in a pseudoischemia pattern on stress PET-CT imaging. *J Nucl Cardiol.* 2016;23:159-60.
3. Rubeaux M, Doris MK, Alessio A, Slomka PJ. Enhancing cardiac PET by motion correction techniques. *Curr Cardiol Rep.* 2017;19:14.
4. Thompson AD, Ficaro EP, Murthy VL, Weinberg RL. Rescued diagnostic quality by motion correction of dynamic cardiac positron emission tomography (PET) perfusion images. *J Nucl Cardiol.* 2019;26:330-2.
5. Klein R, DeKemp RA. Selection of PET camera and implications on the reliability and accuracy of absolute myocardial blood flow quantification. *Curr Cardiol Rep.* 2020;22:109-21. <https://doi.org/10.1007/s11886-020-01376-0>.
6. Büther F, Dawood M, Stegger L, Wübbeling F, Schäfers M, Schober O, et al. List mode-driven cardiac and respiratory gating in PET. *J Nucl Med.* 2009;50:674-81.
7. Lassen ML, Beyer T, Berger A, Beitzke D, et al. Data-driven, projection-based respiratory motion compensation of PET data for cardiac PET/CT and PET/MR imaging. *J Nucl Cardiol.* 2019. <https://doi.org/10.1007/s12350-019-01613-2>.
8. Dawood M, Büther F, Lang N, Schober O, Schäfers KP. Respiratory gating in positron emission tomography: A quantitative comparison of different gating schemes. *Med Phys.* 2007;34:3067-76.
9. Armstrong IS, Memmott MJ, Saint KJ, et al. Assessment of motion correction in dynamic rubidium-82 cardiac PET with and without frame-by-frame adjustment of attenuation maps for calculation of myocardial blood flow. *J Nucl Cardiol.* 2019. <https://doi.org/10.1007/s12350-019-01834-5>.
10. Hunter CRRN, Klein R, Beanlands RS, DeKemp RA. Patient motion effects on the quantification of regional myocardial blood flow with dynamic PET imaging. *Med Phys.* 2016;43:1829-40.
11. Lee BC, Moody JB, Poitrasson-Riviere A, et al. Blood pool and tissue phase patient motion effects on 82-rubidium PET myocardial blood flow quantification. *J Nucl Cardiol.* 2018. <https://doi.org/10.1007/s12350-018-1256-1>.
12. Memmott MJ, Tonge CM, Saint KJ, Arumugam P. Impact of pharmacological stress agent on patient motion during rubidium-82 myocardial perfusion PET/CT. *J Nucl Cardiol.* 2018;25:1286-95.
13. Koenders S, van Dijk J, Jager P, Ottervanger JP, Slump CH, van Dalen JA. Impact of regadenoson induced myocardial creep on dynamic Rubidium-82 PET myocardial blood flow quantification. *J Nucl Cardiol.* 2019;26:719-28.
14. van Dijk JD, Jager PL, Ottervanger JP, Slump CH, van Dalen JA. No need for frame-wise attenuation correction in dynamic Rubidium-82 PET for myocardial blood flow quantification. *J Nucl Cardiol.* 2019. <https://doi.org/10.1007/s12350-019-01654-7>.
15. Vleeming EJ, Lazarenko SV, van der Zant FM, Pan XB, Declerck JM, Wondergem M, et al. Cardiac displacement during 13 N-Ammonia myocardial perfusion PET/CT: Comparison between adenosine and regadenoson induced stress. *J Nucl Med Technol.* 2018;46:114-22.
16. Memmott MJ, Armstrong IS, Hayden C, Arumugam P. Predicting image degradation due to motion in rubidium-82 myocardial perfusion imaging using metrics derived from a novel data-driven motion correction algorithm. 25th Annual Scientific Session and Exhibition of the American Society of Nuclear Cardiology, 2020.
17. DeLong ER, DeLong DM, Clarke-Pearson DL. Comparing the areas under two or more correlated receiver operating characteristic curves: A non-parametric approach. *Biometrics.* 1988;44(3):837-45.
18. Manwell S, Chamberland MJP, Klein R, Xu T, Dekemp R. Evaluation of the clinical efficacy of the PeTrack motion tracking system for respiratory gating in cardiac PET imaging. *Proc. SPIE 10132, Medical Imaging 2017: Physics of Medical Imaging,* 1013251. <https://doi.org/10.1117/12.2255544>.
19. Manwell S, Klein R, Xu T, deKemp RA. Clinical comparison of the Positron Emission Tracking (PeTrack) algorithm with the Real-Time Position Management System for respiratory gating in cardiac positron emission tomography. *Med Phys.* 2019;47:1713-26. <https://doi.org/10.1002/mp.14052>.

**Publisher's Note** Springer Nature remains neutral with regard to jurisdictional claims in published maps and institutional affiliations.